Chapter 1
Tacticity, Regio and Stereoregularity

Giovanni Talarico, Claudio De Rosa and Finizia Auriemma

Contents

Abstract This chapter focus on the polypropylene tacticity. The stereoregularity and regioregularity of the processes catalyzed by heterogeneous and homogeneous Ziegler-Natta catalysts are discussed. The amazing variety of molecular architectures available for polypropylene-based materials are summarized together with the catalytic mechanisms for tacticity control. The main techniques applied for the determination of PP tacticity are reported as well as the outstanding development of new catalyst systems able to achieve unprecedented PP microstructures.

1.1 Introduction

The outstanding performances of polypropylene (PP) market grow continuously and hide the old age of PP which is over sixty. Since the first catalytic synthesis of isotactic polypropylene (iPP) computed in 1954 by using Ziegler catalyst combination

G. Talarico (✉) · C. De Rosa · F. Auriemma
Dipartimento di Scienze Chimiche, Università degli Studi di Napoli Federico II,
Complesso Monte S'Angelo, Via Cintia, 80124 Naples, Italy
e-mail: giovanni.talarico@unina.it

1

$TiCl_4/Al(C_2H_5)_3$ and fractionating the resulting polymer to obtain iPP [1, 2], the global demand growth of iPP continues to be led and is expected to increase from 60 million tons in 2015 to 120 million tons by 2030. The Compound Annual Growth rate (CAGR) is estimated of 5.02% for the forecasted period [3], and the PP market is the second largest polymer business in the world (polyethylene, PE, being the first) making up more than 25% of global polymer demand. Several examples have been reported in literature to give the extend of iPP production for the unaware reader: a suggestive comparison has been reported by Severn et al. [4] who estimated that the iPP production for the 2015 corresponds, in volume, to 24 Khufu's great pyramid at Giza, and the estimate for the 2030 correspond to 41 pyramids!

The heterogeneous Ziegler-Natta (ZN) catalysis has been identified as the best catalytic cycle to produce iPP [5] showing ongoing improvements in catalyst performances from first-generation titanium trichloride catalysts used in the manufacturing processes of the late 1960s to the high activity magnesium chloride supported catalysts used today. The latter systems based on $MgCl_2$ inert support for adsorbing $TiCl_4$ [6] and modified by internal and external donors (ID and ED, respectively), increased the iPP productivity to more than 100 kg (PP)/g(catalyst) and the isotactic index (I.I., defined as the % in mass of polymer insoluble in boiling heptane) to 98–99% [7]. Despite the catalyst generations, the ZN catalysis maintained the essential feature: a combination of a transition-metal (TM) compound with a coordination vacancy and a base-metal alkyl cocatalyst, (typically an aluminium alkyl) which alkylates the TM, generating a metal-carbon bond.

Although heterogeneous ZN catalysts are synonymous of iPP, it is worth to recall that syndiotactic polypropylene (sPP) was first synthesized by using a $TiCl_3$ catalyst [8]. However, this sPP was only a small fraction (less than 10%) of crude polymer mixed together with large amounts of isotactic and atactic polymer and showed low crystallinity. The nature of the active sites is not well known and the mechanism of formation of this polymer is still a matter of debate. The sPP was later directly achieved using vanadium triacetylacetonate and aluminum dialkylmonochloride at fixed Al/V ratio and at very low temperatures [9]. Contrarily to the Ti-isospecific systems, these V-catalysts, promote syndiospecific propagation via secondary (2,1-) insertion of the monomer (see next section). The overall stereo- and regioregularity of the polymer is poor, comprising not only syndiotactic blocks resulting from secondary insertions but also short, atactic blocks arising from sequences of primary insertions. An almost complete control of polypropylene microstructure is achieved by using well-defined single-site homogeneous catalysts based on metallocene [10, 11] and non-metallocene [12, 13] complexes. The PP structures going from highly isotactic to highly syndiotactic semicrystalline structures are now available with properties spanning a range from thermoplastic to elastomeric materials.

These amazing results are due to a (very) lucky combination between PP material properties and coordination catalysis based on TM compounds; the tuning of catalyst active sites framework enhances the intrinsic capability of the simple (and low cost) propene prochiral monomer allowing to obtain (all) the desired microstructures. As we are showing in the following sections, this target has been

achieved thanks to a synergistic action of synthetic efforts, detailed mechanistic studies and advanced experimental techniques.

In this chapter we focus on polypropylene tacticity with a special emphasis on the stereoregularity and regioregularity processes; several microstructures will be discussed together with the mechanisms of stereo and regio control and the main techniques used for their determination.

1.2 Definition and Nomenclature

The catalytic cycle of olefin polymerization via the Cossee mechanism [14] is reported in Fig. 1.1 for the simple case of ethene polymerization. The monomer coordination at the available metal coordination site is followed by monomer insertion into the M-C bond via a four-center transition state (TS), possibly stabilized by α-agostic interaction [15–18], leading to the kinetic product. The next ethene insertion is repeating the same path by coordination at the available site previously occupied by the growing polymer chain (chain migratory mechanism). The model is independent of the active specie charge; it can be applied to neutral active species (as the ones postulated on the surface of heterogeneous ZN catalysts, see path a of Fig. 1.1) [19] or the usually cationic metal-alkyl species (as substantiated by discovery of base free cationic 4 metallocene catalysts) [20–22], in equilibrium with the counterion (A^-) (see path b of Fig. 1.1). In the latter case, the counterion reposition at each insertion step is depending on the ion-couple strength [23–26].

The case of ethene polymerization becomes more complicated for a prochiral monomer like propene, that can insert into the M-C bond in four different ways, (see Fig. 1.2). The structures A and B correspond to a 1,2 propene insertion (the incoming propene monomer binds to the metal atom with the C_1 atom and it is often defined as primary insertion) with two different enantiofaces (*re* and *si*, respectively) whereas the structures C and D correspond to a 2,1 propene insertion (or secondary) with the two enantiofaces *re* and *si*, respectively.[1] Considering that the molecular mass of polypropylene of industrial relevance is on the range of 250 kDa (corresponding to roughly 6000 propene insertion) a single macromolecular chain produced without enantioselectivity control (intending both stereoselectivity and regioselectivity) can be formed by 4^{6000} diasteroisomers!

Let us focus for a moment on catalytic processes in which the regiochemistry of insertion is 1,2 as in the structures A and B of Fig. 1.2: two propene insertions with the same enantioface (e.g. *re* or *si*) generate a sequence with the same configuration of the stereogenic tertiary carbon atom (marked with * in Fig. 1.3 and R = CH$_3$), whereas the insertions of alternate enantiofaces (e.g. *re/si*, or *si/re*) shows opposite
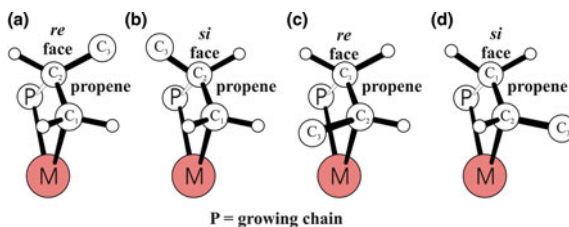
---

[1]In this chapter the nomenclature *si*, *re* is used instead of the nomenclature *R*, *S* as suggested in Corradini and Guerra [27].
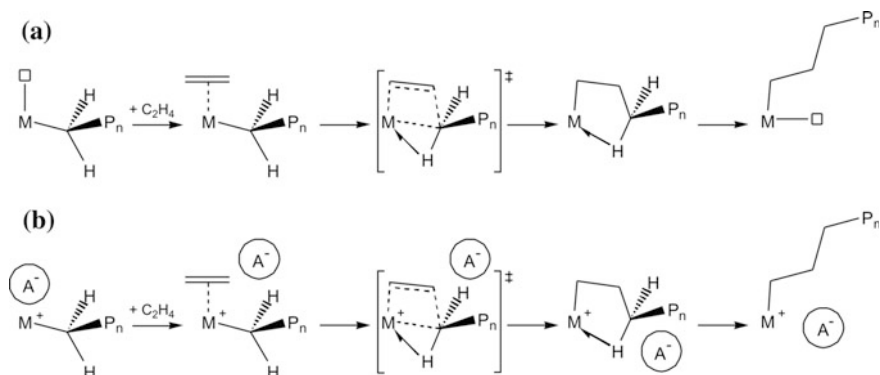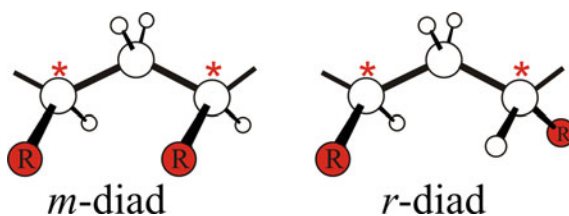
Fig. 1.1 Cossee cycle for **a** neutral and **b** cationic species

Fig. 1.2 Primary or 1,2 (**a**, **b**) and secondary or 2,1 (**c**, **d**) propene insertions into the M-C bond

P = growing chain

Fig. 1.3 Steric diad formed by propene insertion with the same (*m*-diad) and opposite (*r*-diad) enantioface

m-diad   *r*-diad

configurations (see Fig. 1.3). This is said to constitute a *steric diad* and can be labelled as *meso* (abbreviation, *m*) or *racemo* (abbreviation, *r*), respectively.

The common notation used in the field is a saw-horse representation (see top of Fig. 1.4) or modified Fisher projections (see bottom of Fig. 1.4) using horizontal lines to denote polymer backbone bonds, although this does not give the visual impression of the zigzag chain.

Fig. 1.4 Saw-horse (top) and modified (bottom) Fisher projections for *m* and *r* diads


*m*-diad   *r*-diad
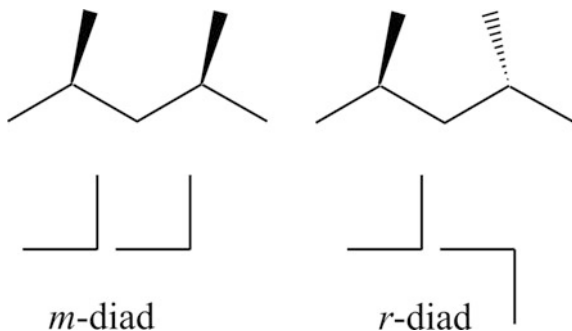
The polypropylene stereostructures can be described in terms of sequences of steric diads. In fact, the arrangement formed by a succession of *m* diads, is defined as isotactic (see Fig. 1.5a), and a sequence of *r* diads is said to be syndiotactic (Fig. 1.5b). In the iPP, the configurational repeating unit is identical with the configurational base unit whereas in the sPP the configurational repeating unit consists of two configurational base units that are enantiomeric [28]. The lack of configurational order lead to an atactic chain (aPP, see Fig. 1.5c); a partial order formed by even monomeric units with the same configuration and all odd ones having a perfectly random configuration (with a dot line in Fig. 1.5d), is called hemiisotactic (hPP). Hemiisotactic polypropylenes represent a very interesting case in the field of macromolecular stereochemistry. Their typical feature is the coexistence of order and disorder: more precisely, order and disorder alternate along the chain in a well-defined way [29].

The stereosequences reported in Fig. 1.5 correspond to idealized definitions and real polypropylene microstructures are more complicated. The presence of configurational or constitutional defects leads to deviations from ideality and such recommended nomenclature can usefully be applied to the predominant structural features of real polymer molecules. Terms as such as "almost completely isotactic" or "highly syndiotactic", are commonly used by polymer scientists although such expressions lack the rigor beloved by the purist [28]. The proper "reading" of PP microstructure is a fundamental source of information not only to deduce the structure/properties relationships but also for understanding the polymerization mechanisms of the catalytic species (a sort of a 'fingerprint'). The typical example is the microstructure achieved with an occasional stereodefect within the isotactic chain reported in Fig. 1.6.

Following the IUPAC recommendations, we should call both A and B structures of Fig. 1.6 as *predominantly isotactic* being the *m* dyads predominant. The *m* sequences are interrupted by two *r* diads (*rr* = triad) in Fig. 1.6a and by one *r* dyad in Fig. 1.6b. At a glance, these two structures show that the single stereodefect (reported in red in Fig. 1.6) is originated by two different mechanisms of stereochemical control. The former shows that the insertion error is corrected by another *r* placement immediately after the first *r* dyad, so that the *m* sequences on both sides
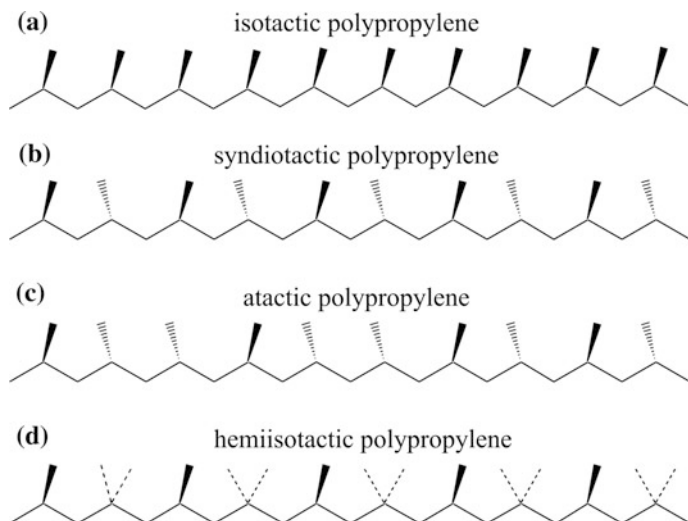
**Fig. 1.5** Polypropylene stereostructures available by TM catalysts
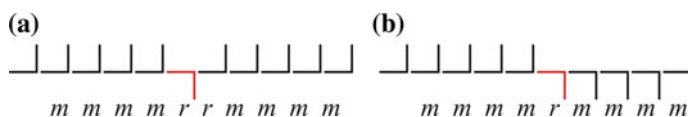
Fig. 1.6 Microstructures of polypropylene synthesized through **a** enantiomorphic site control and **b** chain-end control

of the *rr* placement have the same relative configuration (see Fig. 1.6a). The latter shows that, after a stereochemical insertion, the new configuration is maintained in the propagation until the next insertion error occurs (see Fig. 1.6b).

The first model of stereocontrol is defined as "enantiomorphic site" or chiral site control whereas the second one is defined as "chain-end", depending on the chirality of the last inserted unit in the polymer chain. Two statistical models based on these mechanisms were developed for the interpretation of the observed stereosequence distributions and are known as enantiomorphic-site model [30] and Bernoullian model [31]. Theoretical explanations for the origin of stereocontrol exerted by these two mechanisms will be reported in Sect. 1.4.

Analogous considerations can be extended to the stereodefect effect (in red) of predominantly syndiotactic stereosequences reported in Fig. 1.7.

The syndiotactic control is less straightforward than the isotactic one and needs further details (see Sect. 1.4). Nevertheless, we can assume an enantiomorphic-site control for the structure of Fig. 1.7a whereas some cautions need for a clear-cut assumption to the chain-end control for microstructure reported in Fig. 1.7b.
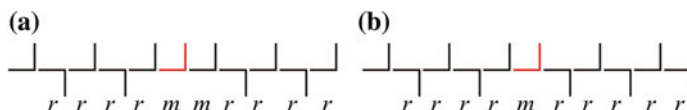
Fig. 1.7 Stereoerror microstructures for propene syndiotactic propagation

The microstructural analysis focused on constitutional defects lead to several microstructures. Heterogeneous ZN catalysts are well known to be highly regioselective in favor of 1,2-insertion of propylene (of the type A and B of Fig. 1.2) and isolated 2,1 enchainment are usually less than 1% [32]. Considering for simplicity an isotactic chain, the isolated 2,1 insertion may produce two different microstructures depending on the inserted enantioface, see Fig. 1.8. We recall that relative configurations at two contiguous carbon atoms in main chains bearing, respectively, substituents a and b (a ≠ b), are designated by the prefix erythro or threo by analogy with the terminology for carbohydrate systems. The presence of regioinverted unit with vicinal methyls in erythro configuration (see Fig. 1.8) means that the 1,2 and 2,1 propene insertions occur with opposite enantioface (see A and D or B and C structures of Fig. 1.2) whereas the threo configuration indicates that the 1,2 and 2,1 propene insertions occur with the same enantioface, (see A and C or B and D structures of Fig. 1.2), respectively.

As a matter of fact, more complicated microstructures are available from experimental data and further details will be reported in the regiochemistry Sect. 1.5.

Overall, all the microstructures reported in Figs. 1.6, 1.7 and 1.8 can be distinguished by ^{13}C-NMR spectra of polypropylenes because the resonance frequencies observed for chemically equivalent carbon nuclei in the solution ^{13}C NMR spectra of polymers are sensitive to the local conformation of the chain. As the conformation is influenced by the microstructure, the solution ^{13}C NMR resonance frequencies of carbon nuclei in polypropylene are sensitive to the microstructure. The large set of polypropylene microstructures obtained by selecting suitable catalysts (and experimental conditions) is, once again, the powerful demonstration of the microstructural control achieved by coordination catalysis guided by an outstanding knowledge of the catalytic mechanisms.
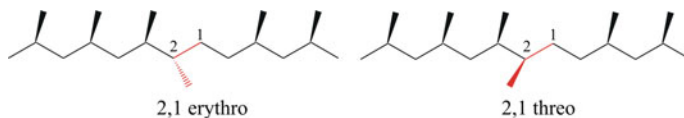

Fig. 1.8 Occasional 2,1 propene insertion in a primary isotactic propagation

1.3 ^{13}C NMR of Polypropylenes

The microstructure of a polymer can best be characterized by nuclear magnetic resonance spectroscopy (NMR) and one-dimensional (ID) proton NMR spectroscopy has made major contributions to the microstructure understanding of synthetic macromolecules. The ^{1}H NMR spectra of typical iPP and sPP are reported in Fig. 1.9.

However, the elective technique for the tacticity analysis of polypropylene samples is the ^{13}C NMR because of the much greater range of ^{13}C chemical shifts with respect to the ^{1}H and consequent greater sensitivity to the (local) structural details. The proton NMR spectroscopy is mainly used for the evaluation of chain-end groups [33–35] or for calculating the total branching level of special polypropylenes promoted by late transition metal (LTM) [36].
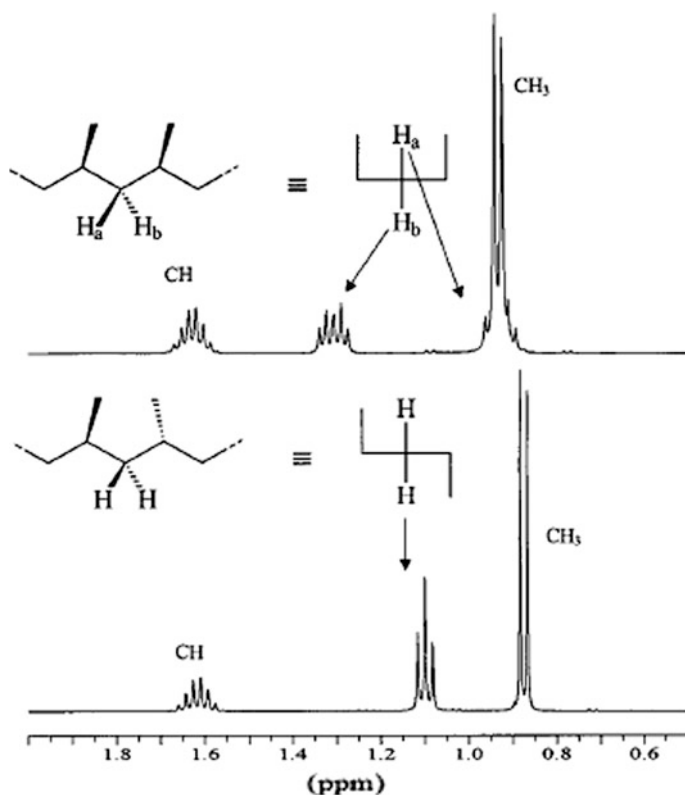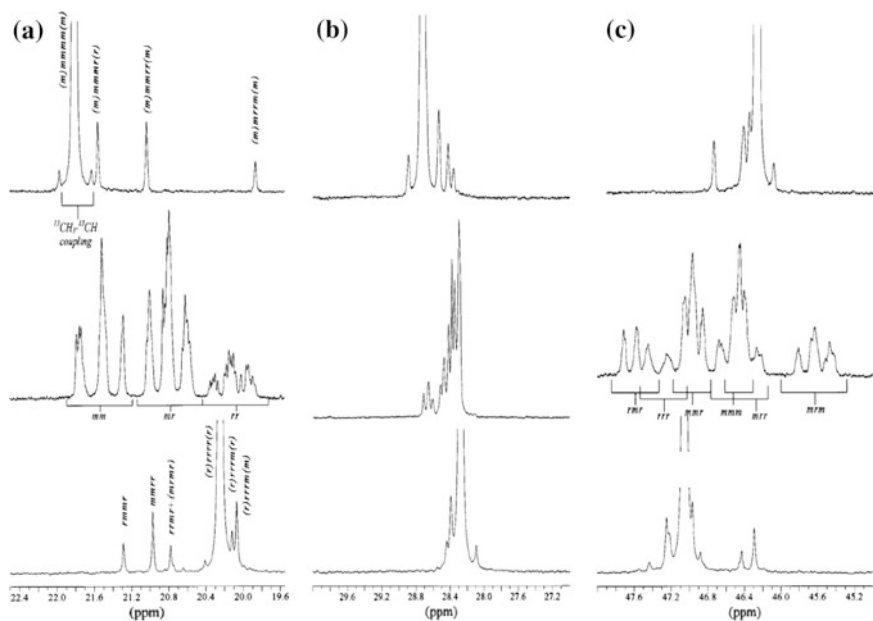

Fig. 1.9 H NMR (400 MHz, C$_2$D$_2$Cl$_4$, 120 °C) of iPP (top) and sPP (bottom). Adapted with permission from Ref. [11]. Copyright (2000) American Chemical Society

In Fig. 1.10, the methyl (A), methine (B) and methylene regions of ^{13}C NMR spectra of representative iPP (top), aPP (middle) and sPP (bottom) samples are reported.

The methyl resonance is split in nine major peaks, (see Fig. 1.10a) assigned to these 10 pentads (the *mmrm* and *rmrr* pentads have the same chemical shift) that is: *mmmm*, *mmmr*, *rmmr*, *mmrr*, *mmrm*, *rmrr*, *mrmr*, *rrrr*, *rrrm* and *mrrm* pentads following the numeration of Fig. 1.11.

The nine bands are divided into three distinct regions corresponding to *mm*, *mr* and *rr* centered pentads (see Fig. 1.10a). Sums of the intensities of the three bands in each region correspond to the *mm*, *mr* and *rr* triads and the PP tacticity can be measured by the contents of triads or pentads, such as [*mm*] or [*mmmm*] for iPP and [*rr*] or [*rrrr*] for sPP. The complete assignment of the polypropylene ^{13}C NMR peaks was a difficult task: the successful approach to the assignment was a well-planned synthesis of accurate model compounds and of polymers of known structure or ^{13}C labeled ones [37] combined with the prediction of the chemical shifts by semiempirical [38, 39] and *γ-gauche* effect methods [40–42].

With improvements in sensitivity and resolution of NMR spectrometers, tactic peaks up to heptad/undecad level have been observed in the methyl carbon region of polypropylenes [43, 44]; hexad/decad level for the methylene [44], and pentad/heptad level for the methine resonances [45, 46]. An excellent review on the use of

Fig. 1.10 The 100 MHz ^{13}C NMR spectra of iPP (top), aPP (middle), and sPP (bottom) for the methyl (**a**); methine (**b**), and methylene (**c**) regions, respectively. Adapted with permission from Ref. [11]. Copyright (2000) American Chemical Society
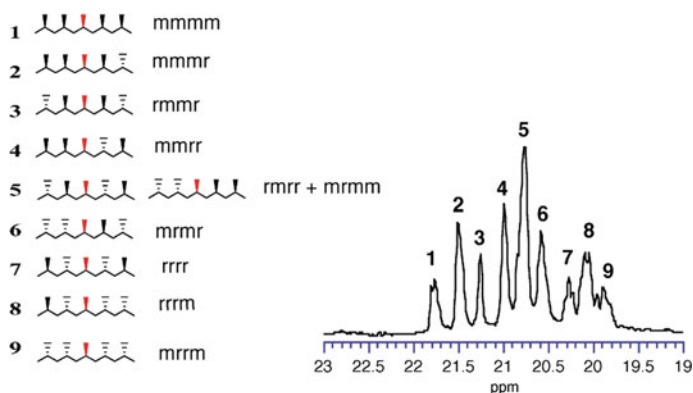
**Fig. 1.11** Assignment of the ten pentads available (left) for the methyl region of ^{13}C NMR spectra (right)

high field ^{13}C NMR spectra for the polypropylene microstructure has been published and the reader who is interested in more detail is referred to [47].

In Fig. 1.12 are reported the high-field 150 MHz ^{13}C NMR spectra for the methyl (left) and methylene (right) regions of four model polypropylene samples: two predominantly iPPs (A and B) with a microstructure-type reported in Fig. 1.6 (A and B); one sPP (C) and one hPP (D). The combination of model compounds prepared with suitable homogeneous catalysts and more refined statistical models allowed a full assignment of spectra like those of Fig. 1.12 [44, 46, 48] with the chemical shift of all peaks. The general protocol for the interpretation of high-field ^{13}C NMR polypropylene spectra has been proposed [44] and insights in several complicated mechanisms of stereocontrol have been obtained [49–52] with a special emphasis on the heterogeneous ZN catalysis [53, 54].

1.4 Steric Defects in PP and Models for Stereocontrol

The assignment of methyl resonances in the ^{13}C NMR spectra allowed the identification of predominant…*mmmmrrmmmm*…-type stereodefects (see Fig. 1.6a) in iPP produced by heterogeneous and homogeneous ZN catalysts. The intensity ratio of the peaks [*mmmr*]:[*mmrr*]:[*mrrm*] = 2:2:1 (Fig. 1.13, top), is in agreement with the enantiomorphic-sites model, which is the more effective control to obtain highly isotactic polypropylenes. A lower isotacticity value is reported for the chain-end control (see Fig. 1.6b) obtained with achiral homogeneous systems at very low polymerization temperature and showing a peak ratio [*mmmr*]:[*mmrm*] = 1:1 (Fig. 1.13, bottom) [55].

The origin of enantiomorphic site control which explain the ^{13}C NMR spectra of Fig. 1.13 (top) was firstly rationalized by Corradini and co-workers by considering nonbonded interactions in the TS of propene insertion for a model of heterogeneous
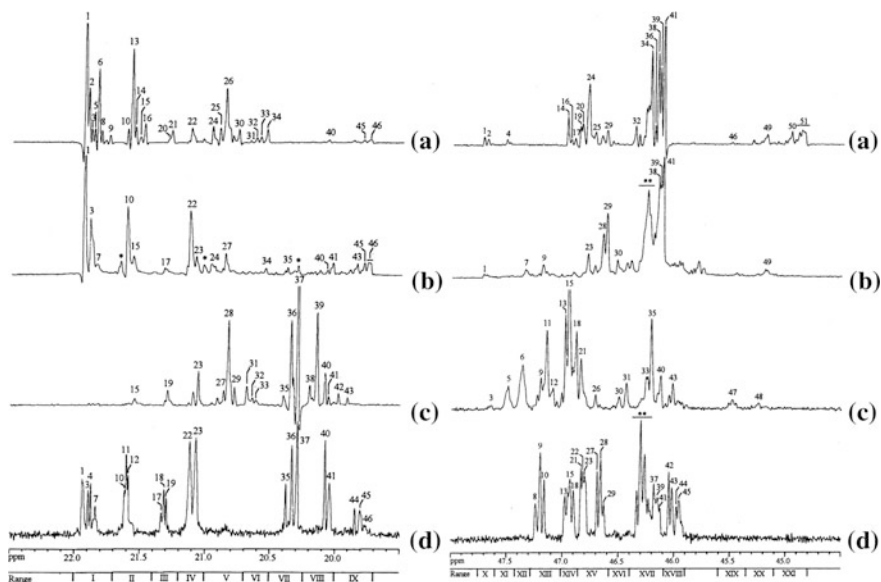
Fig. 1.12 Methyl (left) and methylene (right) regions of the 150 MHz ^{13}C NMR spectra of the four model polypropylene samples **a–d** reported in the text (dissolved in 1,1,2,2-tetrachloroethane-d_2 at 70 °C); δ scale is in ppm downfield of TMS. For peak assignments, see Tables 1–4 reported in Ref. [44]. Adapted with permission from Ref. [44]. Copyright (1997) American Chemical Society

Fig. 1.13 Methyl region of ^{13}C NMR spectra (100 MHz, C$_2$D$_2$Cl$_4$, 120 °C, Ref. *mmmm* at 21.8 ppm) of two iPP samples prepared under enantiomorphic-site control (top) and chain-end control (bottom). Adapted with permission from Ref. [11]. Copyright (2000) American Chemical Society
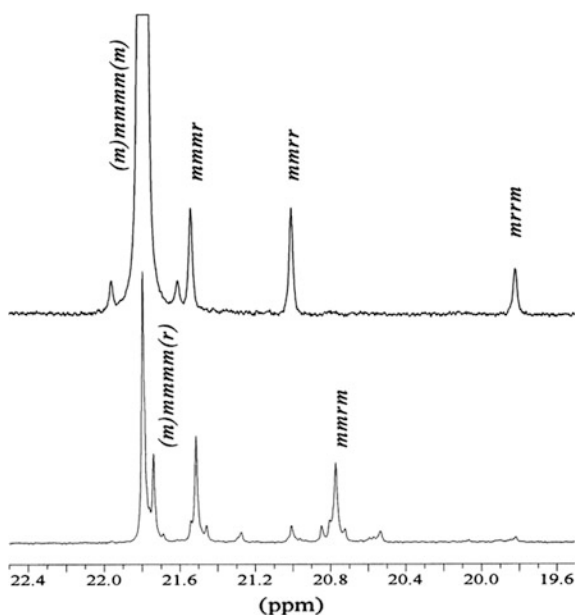
ZN active sites [56–58]. The propene enantioface selection (e.g. *re* preferred to *si* in Fig. 1.14a, b) is dictated by the chirality of active site (e.g. Δ site for octahedral specie in Fig. 1.14 top) which induce a chiral orientation of the growing polymer chain (to avoid steric contact with the ligand framework marked with * in Fig. 1.14b). The oriented growing chain selects the propene enantioface with the methyl group in *anti* to the first C_α-C of the chain to avoid the steric chain-monomer contacts. The same model well explain the isotactic propagation promoted by C_2-symmetric *ansa*-metallocene as estimated by computational methods based on the density functional theory (DFT): in fact, looking at the TS geometries for a
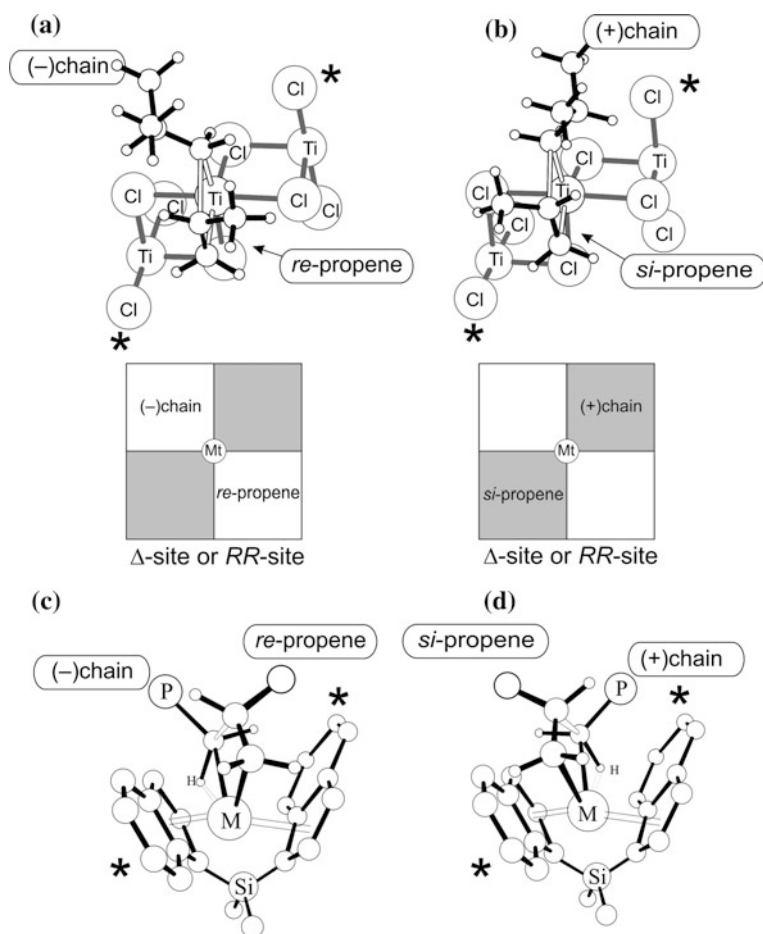
Fig. 1.14 Top: optimized geometries TSs obtained by DFT methods of 1,2 propylene insertion for a C_2-symmetric octahedral Ti model site with Δ configuration (**a**) and for stereoerrors coming from chain misorientation (**b**). Bottom: a similar representation is reported for a prototypical C_2-symmetric *ansa*-metallocene with the *RR* configuration. Middle: the quadrant representation is showing the analogy between these two C_2-symmetric species

prototypical tetrahedral *ansa*-metallocene (see Fig. 1.14 bottom) the lower energetic TS for the structure C with respect to D (which lead to a stereoerror) is due to the right chiral configuration of the growing polymer chain. The role played by the chlorine atoms on heterogeneous surface and the homogeneous ancillary ligand in orienting the growing polymer chain is substantially similar.

The similar origin of isotactic stereoselectivity promoted by heterogeneous and homogeneous systems emerges clearly by using the appropriate quadrant representation (see Fig. 1.14 middle), where the gray quadrants correspond to relatively crowded zones occupied by Cl atoms on top and indenyl ligands on the bottom.

The quadrant representation is a good tool to rationalize the relationship between complex symmetry and polypropylene tacticity. In fact, homogeneous single-site polymerization catalysts can be divided into five symmetry categories reported in Fig. 1.15. The aPP is usually produced by C_{2v}- or C_s-symmetric catalysts that have mirror planes containing the two diastereotopic coordination sites with the same behavior (deviation from ideal aPP may be generated by a chain-end control mechanisms). The sPP is produced by C_s-symmetric catalysts with a mirror plane reflecting the two enantiotopic coordination sites and iPP is produced by C_2-symmetric complexes. More complicated PP architectures can be realized with C_1-asymmetric complexes with diasterotopic coordination sites, ranging from highly to weakly isotactic [59], including isotactic-atactic stereoblock [60] and hemiisotactic [61].

An interesting application of such rules was published by Coates and Waymouth who reported the synthesis of elastomeric PP by using unbridged bis(indenyl) zirconium dichloride bearing bulky phenyl substituents in 2-position of the indenyl moiety. The PP microstructure is formed by isotactic-atactic stereoblocks attributed to changes in the catalyst stereoselectivity during the propagation reaction as schematized in Fig. 1.16.

The syndiospecificity promoted by the typical C_s-symmetric catalyst [62] reported in Fig. 1.17 was indeed the first definitive experimental evidence that Cossee's chain migratory insertion (see Fig. 1.1) was operative. The polymer configurational microstructure is consistent with enantiomorphic-site control, with
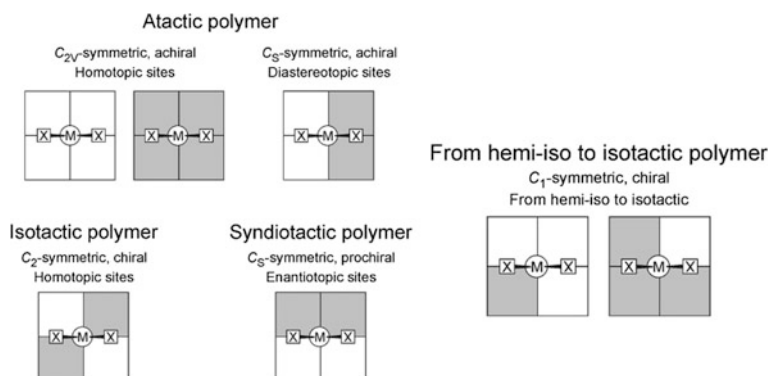
Fig. 1.15 Relationships between catalyst symmetries and polypropylene microstructures achieved
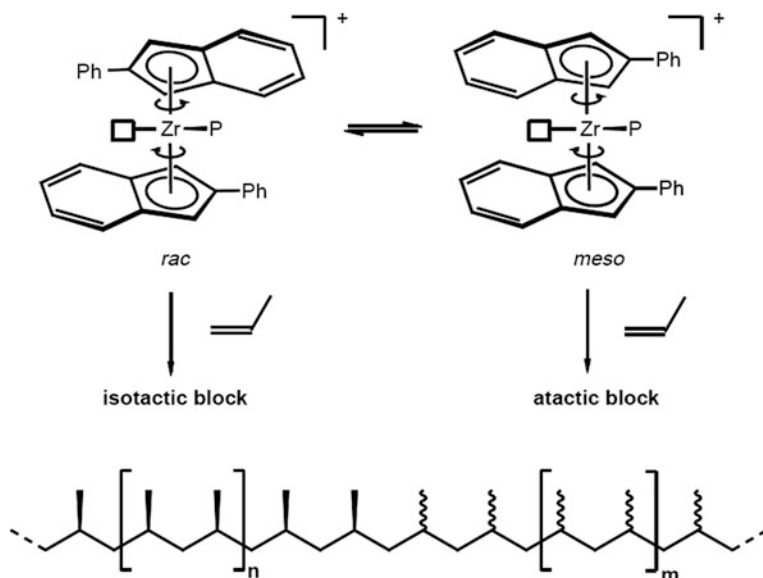
Fig. 1.16 Proposed mechanism for the formation of isotactic–atactic block PP by oscillating catalysts [60]
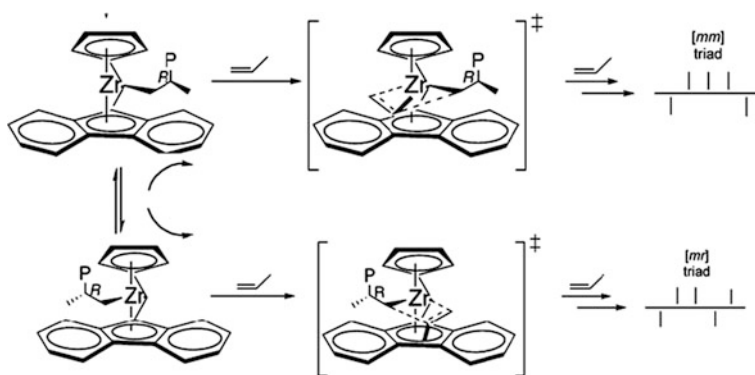
Fig. 1.17 Mechanisms for the formation of stereoerrors generated by the enantiofacial misinsertion (top) and by the site epimerization (SE) (bottom), and their corresponding signature pentad distributions

the active sites isomerizing at each monomer addition. The enantiofacial misinsertion generates the stereodefect with the microstructure of Fig. 1.7a and visualized in Fig. 1.17, top. Occasional skipped insertion of the growing chain before the monomer insertion (often called site epimerization, SE) may also occur, generating instead stereosequences as reported in Fig. 1.17, bottom.

The experimental evidence that the SE error of C_s-*ansa* metallocene catalyst generates a *m*-type stereodefects (see Fig. 1.17, bottom) resembling that of a syndiotactic propagation by chain-end control (see Fig. 1.7b) may induce some confusions on the identification of the right polymerization mechanism. In such cases, the way-out is to examine polypropylene samples prepared in the same experimental conditions but at different propene concentrations ($[C_3H_6]$); in fact, the concentration of *m* defects is expected to increase with decreasing $[C_3H_6]$ under enantiotopic-sites control (see Fig. 1.17, bottom), whereas it is expected to be independent of monomer concentration, in the case of chain-end control.

Finally, remarkable counterion and solvent polarity effects on the stereochemistry of syndiotactic propagation by C_s-*ansa* metallocene have been probed [63]. The ion pairing selection can strongly modulate the relative rates of syndiotactic enchainment versus [*m*], with a marginal effect on [*mm*], which is basically dependent by the catalyst ligand framework. The results are summarized in Fig. 1.18.

As a matter of fact, sPP of high stereoregularity containing only *m*-type of stereodefects have been prepared also with C_2-symmetric bis(phenoxyimine)Ti catalysts [64, 65] (see Fig. 1.19).

The formation of sPP by using a C_2-symmetric catalyst was rather unexpected because of the symmetry rules reported in Fig. 1.15. However, it has been proved by ^{13}C NMR analysis (see Fig. 1.20, top) that these octahedral non-metallocene systems afford highly syndiotactic propagation through 2,1 monomer insertion [66–68] differently from the common 1,2 propagation promoted by C_s-metallocenes (see Fig. 1.20, bottom).

The mechanism for the syndio-selectivity of C_2-octahedral bis(phenoxyimine)Ti complex is not trivial and resembling the one proposed on homogeneous vanadium-based catalytic systems [69]. The secondary chiral growing chain was pivoted to explain the origin of stereoselectivity by dictating the configuration of the fluxional active sites (Δ and Λ), which, in turn, selects the monomer enantiofaces (see Fig. 1.21, reported from Ref. [70]).

These experimental facts highlighted three conclusions: (a) the regiochemistry is an important aspect in particular for PP microstructures revealed by non-metallocene

Fig. 1.18 Stereoerrors for syndiotactic propagation due to the enantioface misinsertion and site isomerization

Fig. 1.19 Methyl region of
^{13}C NMR spectra of sPP
sample synthesized by
C_2-octahedral bis
(phenoxyimine)Ti system
shown in the inset at 0 °C.
Only the *m*-type of stereodefect
is detected [64]

Fig. 1.20 ^{13}C NMR spectra of sPPs obtained by a non-metallocene C_2-octahedral bis(phenoxy-imine)Ti complex (top) and by C_s-metallocene complex (bottom) [67]. The 13–18 and 30–45 ppm regions are attributable to regioirregular units (H = head = CHCH$_3$ moiety; T = tail = CH$_2$ moiety)

Fig. 1.21 Mechanism for syndiotactic propagation of octahedral bis(phenoxyimine) Ti complex. Adapted with permission from Ref. [70]. Copyright (2004) American Chemical Society
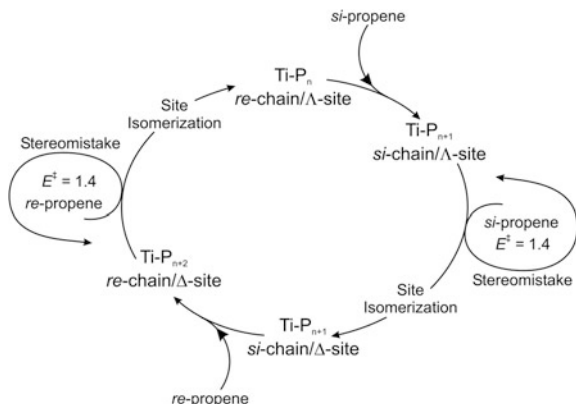
systems (see Sect. 1.5); (b) the impressive development of homogeneous single-site metallocene-based created a large variety of PP microstructure building a consistent dataset to analyze the microstructure/property relationships; (c) the discovery, after the first half of the 1990s, of new generation of non-metallocene catalysts based on Group 4 and LTM enlarged the database of PP microstructure available [12, 13, 71].

1.5 Regio Defects in PP and Models for Regiocontrol

The regiochemistry of propene insertion at heterogeneous ZN catalyst was considered for a long time a minor topic because of the high 1,2 regioselectivity showed by the catalyst. The amount of occasional 2,1 insertion in the iPP chain was so low that needed of special copolymerization techniques with ethene-1-^{13}C/propene to be detected by ^{13}C NMR characterization [32, 72]. Isospecific C_2-metallocene catalysts show a generally lower regioselectivity compared to heterogeneous Ziegler-Natta catalysts: indeed, isolated secondary propene units are often detectable in iPP samples (in a typical range of 0.2–1 mol%) combined with (3,1 units), arising from the unimolecular isomerization of the secondary unit (see Fig. 1.22).

Compared to the C_2-symmetric catalysts, the C_s symmetric ones (see Fig. 1.17) are known to be more regioselective because no regioirregular enchainments are normally detected by ^{13}C NMR in highly syndiotactic polypropylene samples. Because of the remarkable effects that the regiodefects have in the lowering crystallinity and melting point of semicrystalline PP and in the mechanical properties [73, 74] we will discuss them briefly.

A secondary propene insertion in the isotactic propagation can, in principle, generate up to four different regiodefect microstructures (see Fig. 1.23) excluding the isomerization to the 3,1 unit (see Fig. 1.22); two structures come from the (two) enantiofaces of 2,1 inserted unit (see Fig. 1.8) and the other two depend of the absolute configuration of the methyl groups *after* the 2,1 inserted unit (see Fig. 1.23). The conflicting reports in the literature regarding the assignments of the carbon NMR spectrum as well as the stereochemistry of these regio-errors have

Fig. 1.22 Microstructures generated by a propene 2,1 inserted unit
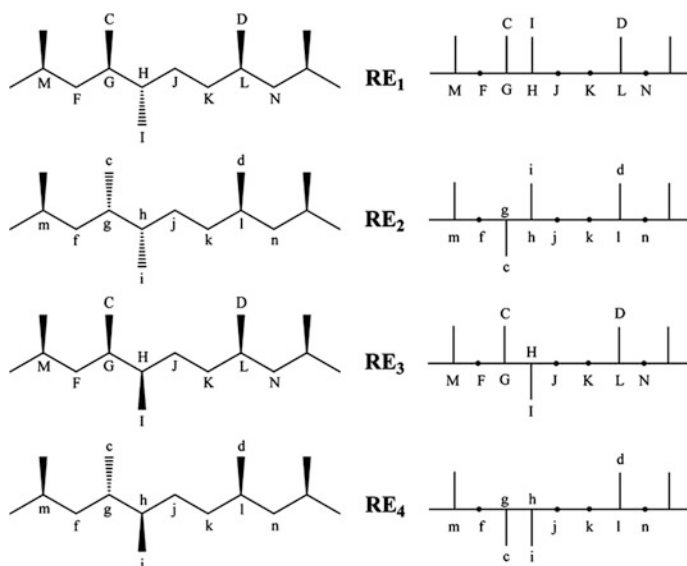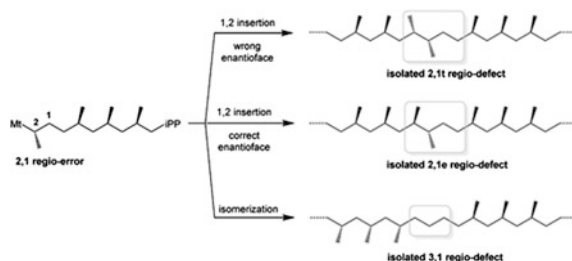
Fig. 1.23 3D structures and Fisher projections of 2,1-insertion regioerrors in iPP. Adapted with permission from Ref. [75]. Copyright (2009) American Chemical Society

been only recently solved by using a high-temperature cryoprobe ^{13}C NMR with much better signal/noise and 2D inadequate [75].

Several experimental and theoretical studies focused on the regiochemistry promoted by *ansa*-metallocene catalysts (for all five symmetry categories reported in Fig. 1.15) leading to the conclusion that the 2,1 insertion is highly

enantioselective for C_2, C_s and C_1 symmetry catalysts (in the last case depending of the catalyst framework), and non-enantioselective for the C_{2v} species. In particular, the 2,1 inserted unit shows the *opposite* enantioface with respect to the 1,2 selected by C_2 and C_1-isospecific site, and the *same* enantioface by C_s-syndiospecific catalyst, respectively. Finally, the 1,2 following the 2,1 insertion occurs with a lower stereoselectivity.

These finding can be easily visualized in Fig. 1.24 looking the lower energetic TS structures for the preferred 1,2 and 2,1 insertions obtained by DFT calculations for the C_2 and C_s *ansa*-metallocene systems, which confirm the above statements.

DFT calculations explained also that, at the opposite of tetrahedral *ansa*-metallocenes, the non-metallocene systems reported in Fig. 1.19, may be easily targeted by electronic factors in a way to modify the ratio between 1,2 and 2,1 insertion [68, 76] so producing the *blocky* structure as the one reported in Fig. 1.25 and detected by ^{13}C NMR spectra of Fig. 1.20 top.
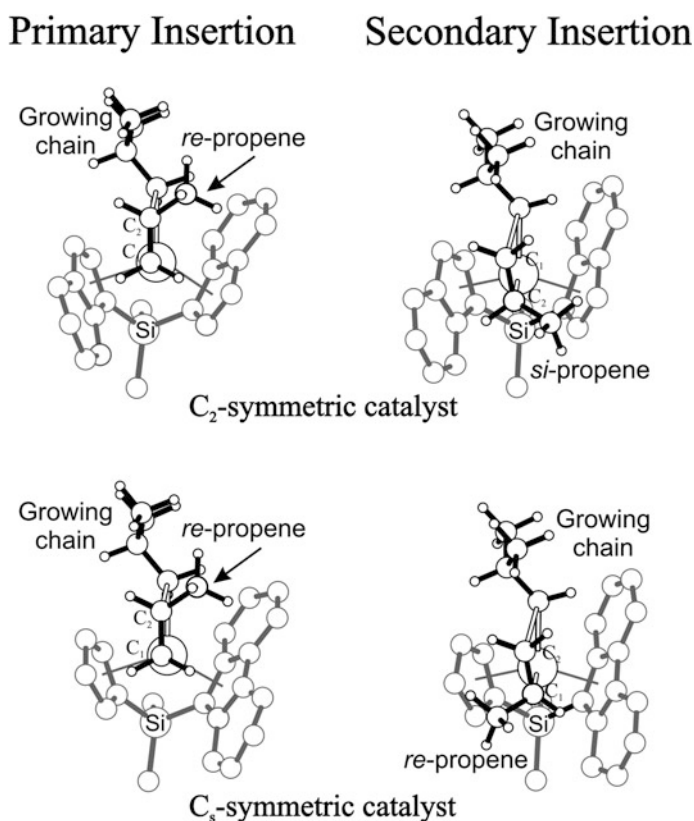
Fig. 1.24 DFT calculated TSs for the preferred 1,2 and 2,1 propene insertions promoted by C_2 (top) and C_s (bottom)-symmetric *ansa*-metallocene species [76]
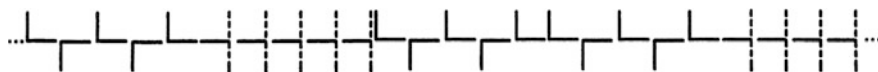
**Fig. 1.25** Blocky microstructure of 2,1 and 1,2 propene insertions obtained with non-metallocene systems

The fine tuning of metallocene systems allowed also the synthesis of new complexes able to promote a highly enantioselective 1,2 insertion *after* the regio-error so obtaining the well-defined microstructure reported in Fig. 1.26. In this way iPP samples with a tailored amount of isolated regiodefects coupled to the absence of *mrrm* or any other chain defect have been prepared. This provides an ideal set of samples for structure–property correlations studies on the effect of such regiodefects on iPP properties [77].

At the same time, the development of new class of non-metallocene catalyst based on pyridyl-amino ligands (see Fig. 1.27, top) enlarged the iPP microstructures set and iPPs of very high stereoregularity with detectable amount of selected 2,1 threo regiodefects are now available (see Fig. 1.27) [78].

The development of new non-metallocene well illustrates the enormous potential of tuning the catalytic properties of different metal centers by their well-defined ligand environment to obtain new and targeted microstructures often by new mechanisms of stereo and regiocontrol [79, 80].
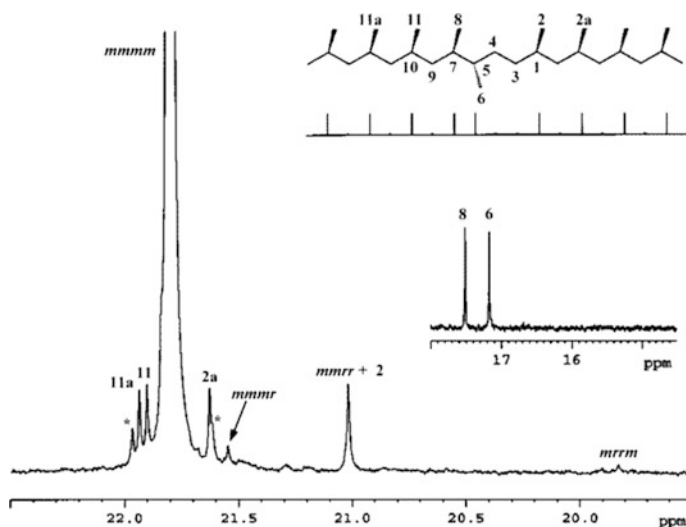
Fig. 1.26 Methyl region of the ^{13}C NMR spectrum of iPP sample produced by a highly stereoselective and not fully regioselective *ansa*-metallocene catalyst, showing the peaks related to 2,1 erythro regiodefects (see Fig. 1.8) and signals corresponding to pentad stereosequences. Adapted with permission from Ref. [73]. Copyright (2005) American Chemical Society
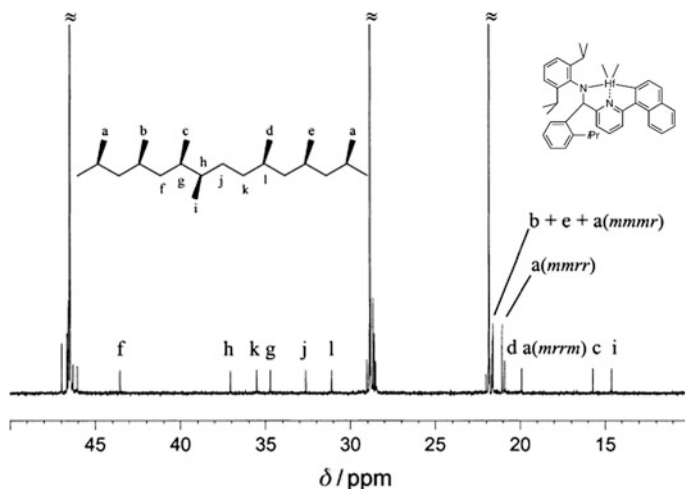
Fig. 1.27 ^{13}C NMR spectrum (100 MHz, (CDCl$_2$)$_2$, 120 °C; δ scale relative to tetramethylsilane at δ = 0 ppm) of the polypropylene sample obtained with a non-metallocene catalyst shown in the inset. The main peaks of the iPP are out of scale. Adapted from Ref. [78]

## 1.6 Heterogeneous Versus Homogeneous ZN Catalysts

The single-site homogeneous catalysts which exhibit more defined microstructures gave a great contribution to the basic understanding of mechanisms and microstructure/property relationship for the PP. However, the large part of industrial iPP production is still demanded to the state-of art heterogeneous catalysts although it is remarkable the growing market for single-site polyolefins with targeted microstructures and controlled molecular weight distributions, especially in gas-phase and slurry-phase polymerization. The superior performances by iPP of heterogeneous (iPP-ZN) with respect to his homogeneous counterpart (iPP-homo) is certainly due to the increased efficiency of the catalyst and the morphology control of the polymer granule, which reduces the reactor fouling [81]. However, the plot reported in Fig. 1.28 highlights some differences in polymer properties; the melting point achieved by iPP-ZN is usually higher than that of the analogous iPP-homo with the same average degree of isotacticity (measured as *mmmm%*).

Significant advances have been made in understanding the fundamental factors determining the performance of multisite MgCl$_2$-supported catalysts. Studies by Busico and co-workers [53, 54, 82] have shown that the chain irregularities in iPP-ZN are not randomly distributed along the chain but are clustered. The chain can therefore contain, in addition to highly isotactic blocks, sequences that can be attributed to less isotactic (isotactoid) and/or to slightly syndiotactic (syndiotactoid) blocks (a schematic example is reported in Fig. 1.29).

It has been suggested that the active site can isomerize very rapidly (during the growth time of a single polymer chain, i.e. in less than a second) between three
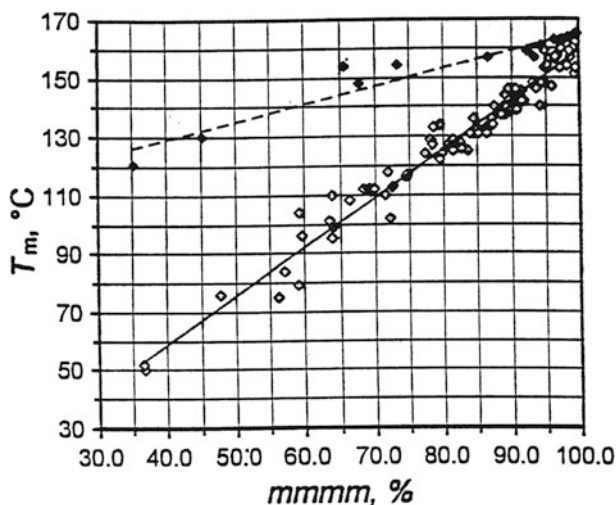
Fig. 1.28 Correlation between % of *mmmm* pentad and DSC melting temperature (T_m; 2nd heating scan) for (predominantly) isotactic polypropylenes. (open diamond) = samples made with metallocene catalysts (from Ref. [11]; (filled diamond) fractions obtained by temperature rising elution fractionation of samples made with heterogeneous Ziegler–Natta catalysts. Adapted from Ref. [47]. Copyright (2001) with permission of Elsevier
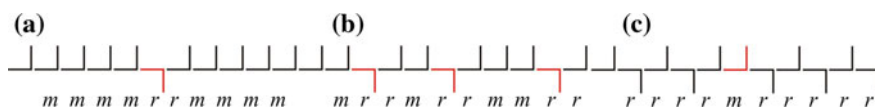
Fig. 1.29 Schematic example of polypropylene microstructure formed by highly isotactic, isotactoid and syndiotactic stereosequences chemically linked

different propagating species. The polymer can therefore be considered to have a stereoblock structure in which highly isotactic sequences alternate with defective isotactoid and/or with syndiotactoid sequences. A mechanistic model (see Fig. 1.30) has been formulated in which the relative contributions of these sequences can be related to site transformations involving the presence or absence of steric hindrance (reported with L1 and L2 in Fig. 1.30) in the vicinity of the active species [53].

Based on these mechanistic assumptions, the various fractions of iPP obtained by fractionation with boiling solvent (e.g. from the diethyl-ether to n-heptane) are characterized by differences in the relative amounts and lengths of these three building blocks. So, the iPP-ZN having *on average* the same % content of steric defects of iPP-homo, will show a higher melting point (see Fig. 1.28) due to longer sequences of chain without defects, as the defects are segregated in the less
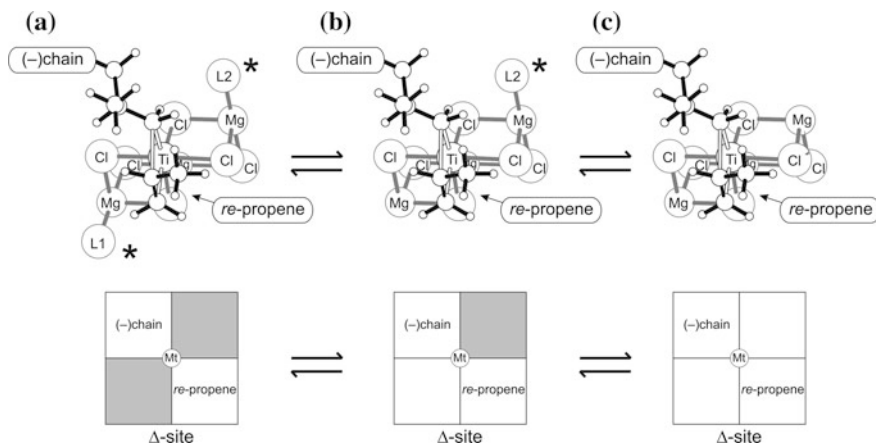
Fig. 1.30 Interconverting three-site model used to explain the stereoblock structures of iPP obtained by ZN heterogeneous catalysts: the site **a** is producing highly isotactic, **b** the isotactoid and **c** the syndiotactic microstructures, respectively. Adapted from Ref. [19]. Copyright (2018) with permission of Elsevier

stereoregular part of the chain. A clear-cut confirmation of these assumptions has been obtained by studying the crystallization behavior of iPPs, because the chain microstructure and the distribution of defects along the polymer strongly influence the polymorphic behavior and, in particular the relative amount of γ form with respect to the α forms (here defined as f_γ). Long regular isotactic sequences of iPP generally crystallize in the α form whereas short isotactic sequences crystallize in the γ form [83, 84]. The amount of γ form developed in the melt-crystallization procedures of model compounds of stereoblock polypropylene samples prepared with the oscillating metallocene catalysts of Fig. 1.16, is much lower than that obtained for iPP-homo samples having the same overall concentration of defects [85]. This suggests that in the stereoblock polypropylene most of the defects are segregated in stereoirregular, noncrystallizable blocks, which alternate to more regular isotactic sequences, long enough to crystallize in the α form. Accordingly, the fact that iPP-ZN largely crystallize in the α form (see Fig. 1.31) as compared to the much higher f_γ value of iPP-homo samples confirms that Ziegler–Natta polypropylenes contain long, almost ideally isotactic sequences along with iso-tactoid sequences which are practically unable to crystallize [86].

The non-random defects distribution has been verified also on iPP samples produced by heterogeneous systems based on Al_2O_3-supported tetraalkyl zirconium catalyst and seems to be related to fast equilibria of the active site modifications on heterogeneous surface [87].

A last remark on the iPP-ZN and iPP-homo differences concerns the number average molecular weight (M_n) and the weight average molecular weight (M_w). The ratio M_w/M_n is called the polydispersity index (PDI) and is an indication of the broadness of molecular weight distribution (MWD). As polydispersity index

Fig. 1.31 Comparison between the relative contents of γ form of iPP, f_γ, as a function of the crystallization temperature T_c for metallocene-made iPP samples and Ziegler-Natta samples T1 and T2 fractionated with boiling solvent, isothermally crystallized from the melt. Adapted with permission from Ref. [86]. Copyright (2004) American Chemical Society
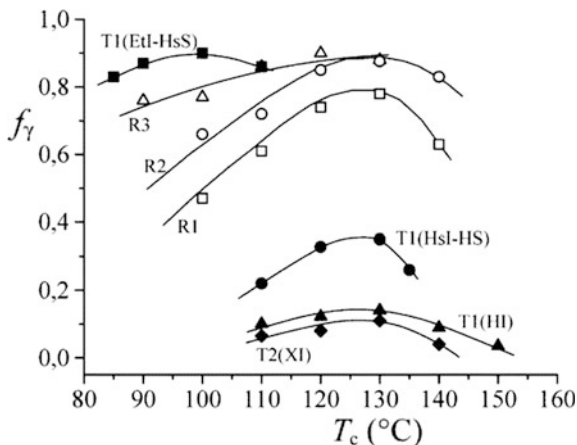
increases, MWD broadens and PDI range from 4–8 for iPP-ZN (typical for multi-site catalysts) whereas iPP-homo show PDI of 2–3 indicating a much narrower MWD (typical of a single-site catalyst).

1.7 Further Techniques for Polypropylene Tacticity Analysis

A large part of the PP tacticity discussion of previous sections was based on ^{13}C NMR analysis. As a matter of fact, there are several experimental techniques whose applications (very often in combination with other techniques) furnish important insights particularly on the microstructure/property relationships. The vibrational spectroscopy is one of the most versatile methods of polymer characterization and Infrared (IR) and Raman spectroscopy probe the vibrational spectrum by absorption and inelastic scattering, respectively. In many cases these two techniques are complementary and can be utilized for determining of the configuration, tacticity and conformation of polymer chains [88]. The great advantage of IR and Raman techniques compared with ^{13}C NMR, analysis is that they are much less time consuming and simpler to perform; IR, indeed, was the first techniques to be used for characterizing the crystallinity of iPP together with the fractionation with boiling solvent [1]. These techniques investigate the crystalline bands (associated with the intermolecular forces occurring between atoms and molecules within the crystalline lattice) and the regularity of helical bands (or regularity bands assigned to intramolecular vibrations within a given chain). As a matter of fact, these methods measure parameters relating to the crystallinity or conformational arrangement of the polypropylene macromolecules and not tacticity itself. For a fast application of the absorption bands at polypropylene samples, the ^{13}C NMR has been used as a calibration method.

For iPP, regularity bands are located below 1400 cm^{-1} and are connected to different values of the number n, which describes the minimum number of monomers linked in an isotactic sequence that defines a helical structure. The IR spectral bands at 1168, 998, 973 and 841 cm^{-1} are related to the formation of regular isotactic helices. The most widely used bands for calibrating the isotacticity (or crystallinity) are the ones at 998 and 841 cm^{-1}. In literature has been reported that they correspond to sequence lengths of 11–12 and 13–14 consecutive repeat units in crystalline, or mesomorphic regions [88]. The band at 973 cm^{-1}, corresponding to five units, can be attributed to both crystalline and amorphous chains in helical conformations and is often used as an internal reference [89]. The connection between these band absorptions and the temperature/crystallinity has been recently demonstrated [89]. The calculation of the A998/A973 ratio from the scanned spectra is straightforward and absorbance ratios A998/A973 and A841/A973 were used as IR stereoregularity parameters of polypropylene [90, 91]. A similar correlation has been found also for sPP; however, the picture is complicated by the fact that semicrystalline sPP samples shows at least three different regular conformations (structural details for this polymer are deeply discussed in the Chap. 2). These regular conformations are all different from the ones in iPP, which makes easy to distinguish between iPP and sPP by IR spectra. The two most common regular sPP conformations, the 2/1helix ($(TTGG)_n$, where T and G stand for gauche and trans conformation of the backbone torsion angles) and the planar zig-zag, can be identified by characteristic bands at 977 and 962 cm^{-1}, respectively. A band at 867 cm^{-1} exists for both conformations and is often used to assess a syndiotacticity index [92] in various combinations. The stereoregularity effects on syndiotactic polypropylene structure have been reviewed by Sevegney et al. [93]. For the characteristics above summarized, the IR spectroscopy is highly recommended for determining the orientation of polypropylene films.

Together with vibrational spectroscopy, the fractionation techniques share the peculiarity to be the oldest methods to be used for understanding the PP tacticity. In the seminal work on the iPP synthesis by Natta was recognized that semicrystalline iPP was insoluble in organic solvents compared to atactic polymer [1].

The most common fractionation technique for iPP samples is based on Soxhlet apparatus where the polymer sample is extracted by using solvents with different boiling points [94]. The heptane is generally accepted as the solvent of choice leading to the standard definition of I.I. Complementary to the I.I, which is an extraction technique, is the xylene insoluble test (XI) which measure the mass of polymer insoluble in xylene after dissolution of the sample and recrystallization. The PP sample is dissolved in hot xylene (135 °C), and by cooling slowly the isotactic fraction can be recrystallized, leaving atactic polymer in solution. Although I.I and XI values are often considered similar, the xylene crystallization is a somewhat more accurate measure of atactic polymer than heptane extractables, because the latter also extracts some low molecular mass isotactic polymer. For most iPP samples prepared with last-generation ZN catalysts the isotactic pentad fraction, *mmmm*, measured by ^{13}C NMR spectra has been found to correlate with xylene insoluble values although similar correlations should be taken with caution.

The measurement of polymer MWD is best done by high temperature gel perme-ation chromatography (GPC) which also provides detailed information on the modality of the molecular weight distribution. GPC separates polymer macro-molecules based on a size exclusion principle whereas for the isolation of discrete molecular weight fractions, a related technique is the two-step process called temperature rising elution fractionation (TREF). In the first step polymer dissolved in a hot o-xylene solution is slowly precipitated by controlled cooling and in the second step the sample is loaded into a thermostated column eluted with a solvent under a stepwise series of increasing temperature conditions. During this phase, polymer fractions sequentially dissolve and each fraction is isolated by reprecipi-tation and then characterized by the available techniques [95, 96]. It is worth to recall that TREF does not strictly fractionate polypropylenes according to tacticity but, instead, according to the longest crystallizable sequences of the chain [97]. Further development of techniques based on the chemical distribution analysis (CCD) lead to the "crystallization analysis fractionation" (CRYSTAF) published by Monrabal [98]. CRYSTAF shares with TREF the same fundamentals on separation according to crystallizability, but the whole fractionation process is carried out during crystallization without support by monitoring the polymer solution con-centration, through the crystallization process while decreasing temperature [99]. Recently, Monrabal et al. [100] proposed a promising technique, called crystal-lization elution fractionation (CEF) which combines the separation power of TREF and CRYSTAF and has been shown to provide very fast analysis of the CCD although CEF analysis still requires expensive specific installation. Overall TREF, CRYSTAF and CEF appear to be powerful techniques for PP tacticity distribution although they can hardly provide quick analysis with common instrument, which is one of the main demands of the manufacturing process operating in large-scale production of polyolefin. The research for further development of fast methods for tacticity analysis is still ongoing [101, 102].

1.8 Polypropylene Microstructures Obtained by Non-metallocene Ligands and by Late Transition Metal

Homogeneous *ansa*-metallocene systems contributed enormously to increase the number of PP microstructure available with the great vantages to produce polypropylenes having controlled desired properties not accessible with commercial iPP produced with heterogeneous Ziegler-Natta catalysts. The range spanned for the PP microstructure are visualized in Fig. 1.32 where only representative cases of synthesized catalysts belonging to the "metallocene revolution" are selected. More details on the (huge) ligand variation based on metallocene skeletons can be found in Refs. [11, 103, 104].
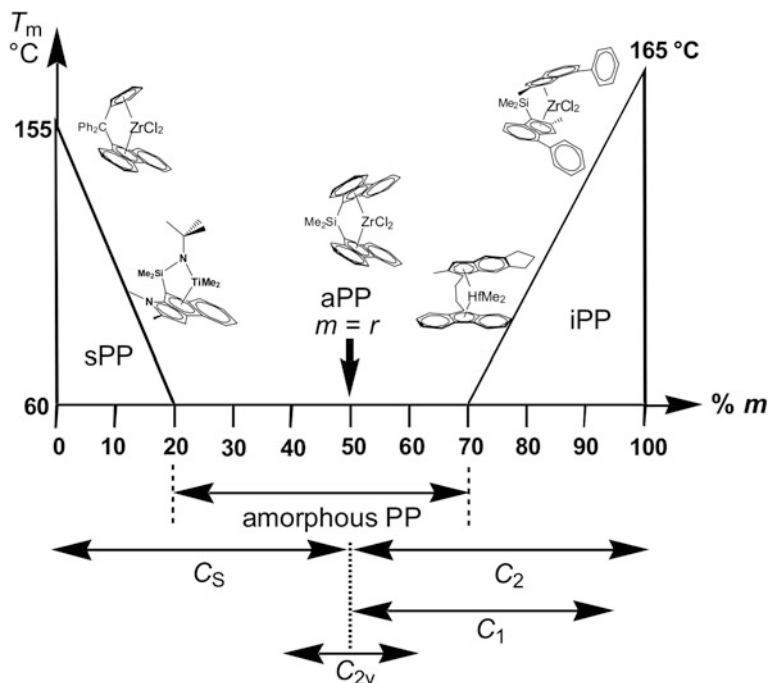
Fig. 1.32 Relationships between catalyst symmetry and PP microstructures available

Research activity in the field of metal-catalyzed olefin polymerization, is still experiencing a significant growth and the number of new catalysts introduced in the last years has provided important developments in the coordination chemistry of transition metals throughout the Periodic Table. The main focus has moved in the achievement of PP microstructures or molecular architectures not available with heterogeneous and homogeneous *ansa*-metallocene systems. Block copolymers (BCP) based on PP are now synthesized by using a living polymerization catalyzed by non-metallocene systems as bis(phenoxy)imine-Ti and pyridylamino-Hf (whose structures are reported in Fig. 1.20, top and Fig. 1.27, respectively) [64, 67, 105–111]. Determining the features that would provide a living system requires further elucidation and works are still in progress [107, 112, 113]; nevertheless, the new molecular architectures reported in Table 1.1 show very interesting and unprecedented properties.

BCPs containing more than one crystallizable block may form nanostructures by microphase separation and self-assembly in lamellar, spherical, and cylindrical microdomains depending on the composition of the BCP [114]. These self-assembled nanostructures with periodicity at the nanoscale level have already shown their potential for fabrication of nanomaterials [115–117]. Very recently a relevant application for multiblock iPP/PE has been disclosed as compatibilizers of iPP and PE blends. The tetrablock copolymers enables morphological control due

Table 1.1 Block copolymer architectures PP-based. With *rir*PP = regioirregular polypropylene

Entry	Block copolymer
1	iPP-*block*-PE
2	iPP-*block*-PE
3	iPP-*block*-poly(E-*co*-P)
4	sPP-*block*-poly(E-*co*-P)
5	sPP-*block*-poly(E-*co*-P)-*block*-sPP
6	sPP-*block*-aPP
7	PE-*block*-poly(E-*co*-P)-*block*-sPP
8	aPP-*block*-PE
9	aPP-*block*-poly(E-*co*-P)
10	iPP-*block*-rirPP
11	iPP-*block*-rirPP-*block*-iPP
12	iPP-*block*-rirPP-*block*-iPP-*rir*PP-*block*-iPP

Adapted from Ref. [105]

to the interfacial compatibilization of phase-separated PE and iPP, so transforming brittle materials into mechanically tough blends [118]. This opens interesting perspectives on recycling the two most common polymers.

The living polymerization approach to synthesize the PP-based BCP architectures suffers the fact that metal complexes only form one polymer chain during the polymerization reaction, rendering the displacement of current commodity polyolefins not applied on industrial scale. Significant and highly promising researches are conducted to develop new strategies for obtaining multiple macromolecular chains per catalyst, such as coordinative chain transfer polymerization (CCTP) [119] or chain shuttling polymerization [120]. The latter one has led to promising results to justify a scale-up to industrial process. In this strategy two different catalysts which behave differently in the olefin polymerization are used. A chain shuttling agent transfers the polymer chain from one catalyst to other forming BCPs having segments of different microstructures. In this way BCPs combining different mechanical properties, due to the different microstructures, in one polymer are prepared.

At the same time, successful new classes of highly active non-metallocene catalysts including LTM such as the Ni and Pd diimine catalysts [121], or the Fe bis (imino)pyridyl catalysts are reported [122]. All of them are showing peculiar PP microstructures, mainly because all possible combinations of regio-chemistries and stereo-chemistries have been observed in propylene polymerization.

1.9 Concluding Remarks

The tacticity of polypropylenes has revealed to be always a "hot" topic although more than sixty years are passed from the discovery of its first crystalline form by metal-catalyzed olefin polymerization. The success of the PP is due to for a large part to serendipity of catalyst discoveries and hard empirical works that make the

research activity in this field still attracting for scientists and experiencing a significant growth. In this chapter we tried to summarize the amazing variety of PP microstructures available with TM catalysts. The next important targets for expanding the PP tacticity are already fixed: (a) the functionalization of PP-based materials with polar groups by using catalysts able to promote copolymerization with polar comonomers in good catalytic activity; (b) the synthesis of tuned PP-based BCPs with activity on the scale for industrial applications.

Undoubtedly, the future will witness continued research of organometallic chemistry and polymer science to achieve new PP microstructures for targeted applications. This is, for sure, not the end of the story.

References

1. Natta G, Pino P, Corradini P et al (1955) Crystalline high polymers of α-olefins. J Am Chem Soc 77:1708–1710. https://doi.org/10.1021/ja01611a109
2. Natta G (1955) Une nouvelle classe de polymeres d'α-olefines ayant une régularité de structure exceptionnelle. J Polym Sci 16:143–154. https://doi.org/10.1002/pol.1955.120168205
3. (2014) News provided by MarketOptimizer.org. https://www.prnewswire.com/news-releases/global-polypropylene-market-capacity-to-see-58-cagr-to-2018-says-a-new-research-report-available-with-marketoptimizerorg-268474302.html
4. Severn JR, Chadwick JC, Duchateau R et al (2006) "Bound but not gagged"—immobilizing single-site α-olefin polymerization catalysts. Chem Rev 105:4073–4147. https://doi.org/10.1021/cr040670d
5. Moore EP Jr (1996) Polypropylene handbook: polymerization, characterization, properties, processing, applications. Hanser Publishers, Munich
6. Kashiwa N (2004) The discovery and progress of $MgCl_2$-supported $TiCl_4$ catalysts. J Polym Sci A Polym Chem 42:1–8. https://doi.org/10.1002/pola.10962
7. Chadwick JC (2009) Polyolefins—catalyst and process innovations and their impact on polymer properties. Macromol React Eng 3:428-432. https://doi.org/10.1002/mren.200900043
8. Natta G, Pasquon I, Corradini P et al (1961) Alti polimeri lineari del propilene aventi struttura sindiotattica. Rend Acc Naz Lincei 28:539–544
9. Natta G, Pasquon I, Zambelli A (1962) Stereospecific catalysts for the head-to-tail polymerization of propylene to a crystalline syndiotactic polymer. J Am Chem Soc 84:1488–1490. https://doi.org/10.1021/ja00867a029
10. Brintzinger H-H, Fischer D, Mülhaupt R (1995) Stereospecific olefin polymerization with chiral metallocene catalysts. Angew Chem Int Edit 34:1143–1170. https://doi.org/10.1002/anie.199511431
11. Resconi L, Cavallo L, Fait A (2000) Selectivity in propene polymerization with metallocene catalysts. Chem Rev 100:1253–1346. https://doi.org/10.1021/cr9804691
12. Gibson VC, Spitzmesser SK (2003) Advances in non-metallocene olefin polymerization catalysis. Chem Rev 103:283–315. https://doi.org/10.1021/cr980461r
13. Baier MC, Zuideveld MA, Mecking S (2014) Post-metallocenes in the industrial production of polyolefins. Angew Chem Int Edit 53:9722–9744. https://doi.org/10.1002/anie.201400799

14. Cossee P (1964) Ziegler-Natta catalysis I. Mechanism of polymerization of α-olefins with Ziegler-Natta catalysts. J Catal 3:80–88. https://doi.org/10.1016/0021-9517(64)90095-8

15. Brookhart M, Green MLH, Wong LL (1988) Carbon-hydrogen-transition metal bonds. Prog Inorg Chem 36:1–124 https://doi.org/10.1002/9780470166376.ch1

16. Krauledat H, Brintzinger HH (1990) Isotope effects associated with α-olefin insertion in zirconocene-based polymerisation catalysts: evidence for an α-agostic transition state. Angew Chem Int Edit 29:1412–1413. https://doi.org/10.1002/anie.199014121

17. Grubbs RH, Coates GW (1996) α-agostic interactions and olefin insertion in metallocene polymerization catalysts. Acc Chem Res 29:85–93. https://doi.org/10.1021/ar9501683

18. Talarico G, Budzelaar PHM (2016) α-agostic interactions and growing chain orientation for olefin polymerization catalysts. Organometallics 35:47–54. https://doi.org/10.1021/acs.organomet.5b00866

19. Bahri-Laleh N, Hanifpour A, Mirmohammadi SA et al (2018) Computational modeling of heterogeneous Ziegler-Natta catalysts for olefins polymerization. Prog Polym Sci 84:89–114. https://doi.org/10.1016/j.progpolymsci.2018.06.005

20. Eisch JJ, Piotrowski AM, Brownstein SK et al (1985) Organometallic compounds of group III. Part 41. Direct observation of the initial insertion of an unsaturated hydrocarbon into the titanium-carbon bond of the soluble ziegler polymerization catalyst Cp_2TiCl_2-MeAlCl$_2$. J Am Chem Soc 107:7219–7221. https://doi.org/10.1021/ja00310a100

21. Jordan RF, Bajgur CS, Willett R et al (1986) Ethylene polymerization by a cationic dicyclopentadienyl zirconium(iv) alkyl complex. J Am Chem Soc 108:7410–7411. https://doi.org/10.1021/ja00283a047

22. Jordan RF (1991) Chemistry of cationic dicyclopentadienyl group 4 metal-alkyl complexes. In Stone FGA, West R (eds) Advances in organometallic chemistry, vol 32. Academic Press, pp 325–387. https://doi.org/10.1016/S0065-3055(08)60482-7

23. Chen EY-X, Marks TJ (2000) Cocatalysts for metal-catalyzed olefin polymerization: activators, activation processes, and structure-activity relationships. Chem Rev 100:1391–1434. https://doi.org/10.1021/cr980462j

24. Mohammed M, Nele M, Al-Humydi A et al (2003) Counterion effects on propylene polymerization using two-state ansa-metallocene complexes. J Am Chem Soc 125:7930–7941. https://doi.org/10.1021/ja0207706

25. Correa A, Cavallo L (2006) Dynamic properties of metallocenium ion pairs in solution by atomistic simulations. J Am Chem Soc 128:10952–10959. https://doi.org/10.1021/ja062407v

26. Rocchigiani L, Ciancaleoni G, Zuccaccia C et al (2011) Low-temperature kinetic NMR studies on the insertion of a single olefin molecule into a Zr-C bond: Assessing the counterion–solvent interplay. Angew Chem Int Edit 50:11752–11755. https://doi.org/10.1002/anie.201105122

27. Corradini P, Guerra G (1991) Models for the stereospecificity in homogeneous and heterogeneous Ziegler-Natta polymerizations. Prog Polym Sci 16:239–257. https://doi.org/10.1016/0079-6700(91)90018-G

28. Jones RG, Wilks ES, Val Metanomski W et al (2009) Compendium of polymer terminology and nomenclature: IUPAC recommendations 2008. Royal Society of Chemistry

29. Farina M, Di Silvestro G, Sozzani P (1991) Hemitactic polymers. Prog Polym Sci 16:219–238. https://doi.org/10.1016/0079-6700(91)90017-F

30. Shelden RA, Fueno T, Tsunetsugu T et al (1965) A one-parameter model for isotactic polymerization based on enantiomorphic catalyst sites. J Polym Sci Pol Lett 3:23–26. https://doi.org/10.1002/pol.1965.110030107

31. Bovey FA, Tiers GVD (1960) Polymer NSR spectroscopy. II. The high resolution spectra of methyl methacrylate polymers prepared with free radical and anionic initiators. J Polym Sci 44:173–182. https://doi.org/10.1002/pol.1960.1204414315

32. Busico V, Chadwick JC, Cipullo R et al (2004) Propene/ethene-[1-13c] copolymerization as a tool for investigating catalyst regioselectivity. $MgCl_2$/internal donor/$TiCl_4$ − external donor/AlR_3 systems. Macromolecules 37:7437–7443. https://doi.org/10.1021/ma049104a

33. Leclerc MK, Brintzinger HH (1996) Zr − alkyl isomerization in ansa-zirconocene-catalyzed olefin polymerizations. Contributions to stereoerror formation and chain termination. J Am Chem Soc 118:9024–9032. https://doi.org/10.1021/ja961157n

34. Resconi L (1999) On the mechanisms of growing-chain-end isomerization and transfer reactions in propylene polymerization with isospecific, C2-symmetric zirconocene catalysts. J Mol Catal A-Chem 146:167–178. https://doi.org/10.1016/S1381-1169(99)00101-6

35. Resconi L, Camurati I, Sudmeijer O (1999) Chain transfer reactions in propylene polymerization with zirconocene catalysts. Top Catal 7:145–163. https://doi.org/10.1023/a:1019115801193

36. McCord EF, McLain SJ, Nelson LTJ et al (2007) ^{13}C NMR analysis of α-olefin enchainment in poly(α-olefins) produced with nickel and palladium α-diimine catalysts. Macromolecules 40:410–420. https://doi.org/10.1021/ma061547m

37. Zambelli A, Locatelli P, Bajo G et al (1975) Model compounds and ^{13}C NMR observation of stereosequences of polypropylene. Macromolecules 8:687–689. https://doi.org/10.1021/ma60047a024

38. Grant DM, Paul EG (1964) Carbon-13 magnetic resonance. II. Chemical shift data for the alkanes. J Am Chem Soc 86:2984–2990. https://doi.org/10.1021/ja01069a004

39. Lindeman LP, Adams JQ (1971) Carbon-13 nuclear magnetic resonance spectrometry. Chemical shifts for the paraffins through C9. Anal Chem 43:1245–1252. https://doi.org/10.1021/ac60304a002

40. Schilling FC, Tonelli AE (1980) Carbon-13 nuclear magnetic resonance of atactic polypropylene. Macromolecules 13:270–275. https://doi.org/10.1021/ma60074a013

41. Zambelli A, Locatelli P, Provasoli A et al (1980) Correlation between ^{13}C NMR chemical shifts and conformation of polymers. 3. Hexad sequence assignments of methylene spectra of polypropylene. Macromolecules 13:267–270. https://doi.org/10.1021/ma60074a012

42. Cheng HN, Lee GH (1987) ^{13}C NMR assignments of the methylene carbons in polypropylene. Macromolecules 20:436–438. https://doi.org/10.1021/ma00168a038

43. Hayashi T, Inoue Y, Chûjô R et al (1988) Heptad configurational analysis of ^{13}C NMR spectra in highly isotactic polypropylene. Polymer 29:138–143. https://doi.org/10.1016/0032-3861(88)90213-3

44. Busico V, Cipullo R, Monaco G et al (1997) Full assignment of the 13C NMR spectra of regioregular polypropylenes: methyl and methylene region. Macromolecules 30:6251–6263. https://doi.org/10.1021/ma970466a

45. Miyatake T, Kawai Y, Seki Y et al (1989) ^{13}C NMR assignments of the methine carbons in polypropylene using two-dimensional ^{13}C-^{13}C inadequate NMR spectroscopy. Polym J 21:809–814. https://doi.org/10.1295/polymj.21.809

46. Busico V, Cipullo R, Monaco G et al (1998) Full assignment of the 13C NMR spectra of regioregular polypropylenes: methine region. Macromolecules 31:8713–8719. https://doi.org/10.1021/ma981040e

47. Busico V, Cipullo R (2001) Microstructure of polypropylene. Prog Polym Sci 26:443–533. https://doi.org/10.1016/S0079-6700(00)00046-0

48. Busico V, Cipullo R, Corradini P et al (1995) Advances in the ^{13}C NMR microstructural characterization of propene polymers. Macromolecules 28:1887–1892. https://doi.org/10.1021/ma00110a024

49. Busico V, Van Axel Castelli V, Aprea P et al (2003) "Oscillating" metallocene catalysts: what stops the oscillation? J Am Chem Soc 125:5451–5460. https://doi.org/10.1021/ja0284557

50. Busico V, Cipullo R, Kretschmer WP et al (2002) "Oscillating" metallocene catalysts: how do they oscillate? Angew Chem Int Edit 41:505–508. https://doi.org/10.1002/1521-3773(20020201)41:3%3c505::AID-ANIE505%3e3.0.CO;2-J

51. Busico V, Cipullo R, Kretschmer WP et al (2002) The strange case of the "oscillating" catalysts. Macromol Symp 189:127–141. https://doi.org/10.1002/masy.200290002

52. Busico V, Cipullo R, Cutillo F et al (2003) Syndiotactic poly(propylene) from [me₂si(3,6-di-tert-butyl-9-fluorenyl)(n-tert-butyl)]TiCl₂–based catalysts: Chain-end or enantiotopic-sites stereocontrol? Macromol Chem Phys 204:1269–1274. https://doi.org/10.1002/macp.200390095

53. Busico V, Cipullo R, Monaco G et al (1999) High-resolution ^{13}C NMR configurational analysis of polypropylene made with MgCl$_2$-supported Ziegler-Natta catalysts. 1. The "model" system MgCl$_2$/TiCl$_4$-2.6- dimethylpyridine/Al(C$_2$H$_5$)$_3$. Macromolecules 32:4173–4182. https://doi.org/10.1021/ma981941n

54. Busico V, Cipullo R, Talarico G et al (1997) New evidence on the nature of the active sites in heterogeneous Ziegler − Natta catalysts for propene polymerization. Macromolecules 30:4786–4790. https://doi.org/10.1021/ma9704673

55. Ewen JA (1984) Mechanisms of stereochemical control in propylene polymerizations with soluble group 4b metallocene/methylalumoxane catalysts. J Am Chem Soc 106:6355–6364. https://doi.org/10.1021/ja00333a041

56. Corradini P, Barone V, Fusco R et al (1979) Analysis of models for the Ziegler-Natta stereospecific polymerization on the basis of non-bonded interactions at the catalytic site—I. The Cossee model. Eur Polym J 15:1133–1141. https://doi.org/10.1016/0014-3057(79)90048-X

57. Corradini P, Guerra G, Fusco R et al (1980) Analysis of models for the Ziegler-Natta stereospecific polymerization on the basis of non-bonded interactions at the catalytic site—II: edges, steps and reliefs on the surface of layered modifications of TiCl$_3$. Eur Polym J 16:835–842. https://doi.org/10.1016/0014-3057(80)90113-5

58. Corradini P, Barone V, Fusco R et al (1982) Steric control in Ziegler-Natta catalysts: an analysis of nonbonded interactions at model catalytic sites. J Catal 77:32–42. https://doi.org/10.1016/0021-9517(82)90143-9

59. Guerra G, Cavallo L, Moscardi G et al (1996) Back-skip of the growing chain at model complexes for the metallocene polymerization catalysis. Macromolecules 29:4834–4845. https://doi.org/10.1021/ma951743l

60. Coates GW, Waymouth RM (1995) Oscillating stereocontrol: a strategy for the synthesis of thermoplastic elastomeric polypropylene. Science 267:217–219. https://doi.org/10.1126/science.267.5195.217

61. Farina M, Di Silvestro G, Sozzani P (1993) Hemiisotactic polypropylene: a key point in the elucidation of the polymerization mechanism with metallocene catalysts. Macromolecules 26:946–950. https://doi.org/10.1021/ma00057a010

62. Ewen JA, Jones RL, Razavi A et al (1988) Syndiospecific propylene polymerizations with Group IVB metallocenes. J Am Chem Soc 110:6255–6256. https://doi.org/10.1021/ja00226a056

63. Chen M-C, Roberts JAS, Marks TJ (2004) Marked counteranion effects on single-site olefin polymerization processes. Correlations of ion pair structure and dynamics with polymerization activity, chain transfer, and syndioselectivity. J Am Chem Soc 126:4605–4625. https://doi.org/10.1021/ja036288k

64. Tian J, Hustad PD, Coates GW (2001) A new catalyst for highly syndiospecific living olefin polymerization: homopolymers and block copolymers from ethylene and propylene. J Am Chem Soc 123:5134–5135. https://doi.org/10.1021/ja0157189

65. Saito J, Mitani M, Mohri J-I et al (2001) Highly syndiospecific living polymerization of propylene using a titanium complex having two phenoxy-imine chelate ligands. Chem Lett 30:576–577. https://doi.org/10.1246/cl.2001.576

66. Hustad PD, Tian J, Coates GW (2002) Mechanism of propylene insertion using bis (phenoxyimine)-based titanium catalysts: An unusual secondary insertion of propylene in a Group IV catalyst system. J Am Chem Soc 124:3614–3621. https://doi.org/10.1021/ja0122593

67. Mitani M, Furuyama R, Mohri J-I et al (2003) Syndiospecific living propylene polymerization catalyzed by titanium complexes having fluorine-containing phenoxy − imine chelate ligands. J Am Chem Soc 125:4293–4305. https://doi.org/10.1021/ja029560j

68. Talarico G, Busico V, Cavallo L (2003) Origin of the regiochemistry of propene insertion at octahedral column 4 polymerization catalysts: design or serendipity? J Am Chem Soc 125:7172–7173. https://doi.org/10.1021/ja029604o

69. Corradini P, Guerra G, Pucciariello R (1985) New model of the origin of the stereospecificity in the synthesis of syndiotactic polypropylene. Macromolecules 18:2030–2034. https://doi.org/10.1021/ma00152a039

70. Corradini P, Guerra G, Cavallo L (2004) Do new century catalysts unravel the mechanism of stereocontrol of old Ziegler-Natta catalysts? Accounts Chem Res 37:231–241. https://doi.org/10.1021/ar030165n

71. Makio H, Terao H, Iwashita A et al (2011) FI catalysts for olefin polymerization–a comprehensive treatment. Chem Rev 111:2363–2449. https://doi.org/10.1021/cr100294r

72. Busico V, Cipullo R, Polzone C et al (2003) Propene/ethene-[1-13C] copolymerization as a tool for investigating catalyst regioselectivity. 2. The $MgCl_2/TiCl_4 - AlR_3$ system. Macromolecules 36:2616–2622. https://doi.org/10.1021/ma034138o

73. De Rosa C, Auriemma F, Paolillo M et al (2005) Crystallization behavior and mechanical properties of regiodefective, highly stereoregular isotactic polypropylene: effect of regiodefects versus stereodefects and influence of the molecular mass. Macromolecules 38:9143–9154. https://doi.org/10.1021/ma051004x

74. De Rosa C, Auriemma F, Di Capua A et al (2004) Structure − property correlations in polypropylene from metallocene catalysts: stereodefective, regioregular isotactic polypropylene. J Am Chem Soc 126:17040–17049. https://doi.org/10.1021/ja045684f

75. Zhou Z, Stevens JC, Klosin J et al (2009) NMR study of isolated 2,1-inverse insertion in isotactic polypropylene. Macromolecules 42:2291–2294. https://doi.org/10.1021/ma802770f

76. Correa A, Talarico G, Cavallo L (2007) Regiochemistry of propene insertion with Group 4 polymerization catalysts from a theoretical perspective. J Organomet Chem 692:4519–4527. https://doi.org/10.1016/j.jorganchem.2007.04.015

77. Reichelt K, Parkinson M, Resconi L (2016) Influence of temperature on the regioselectivity of highly isospecific C_2-symmetric zirconocenes in propene polymerization. Macromol Chem Phys 217:2415–2430. https://doi.org/10.1002/macp.201600088

78. Boussie TR, Diamond GM, Goh C et al (2006) Nonconventional catalysts for isotactic propene polymerization in solution developed by using high-throughput-screening technologies. Angew Chem Int Edit 45:3278–3283. https://doi.org/10.1002/anie.200600240

79. Domski GJ, Eagan JM, De Rosa C et al (2017) Combined experimental and theoretical approach for living and isoselective propylene polymerization. ACS Catal 7:6930–6937. https://doi.org/10.1021/acscatal.7b02107

80. De Rosa C, Di Girolamo R, Talarico G (2016) Expanding the origin of stereocontrol in propene polymerization catalysis. ACS Catal 6:3767–3770. https://doi.org/10.1021/acscatal.6b00863

81. Simonazzi T, Cecchin G, Mazzullo S (1991) An outlook on progress in polypropylene-based polymer technology. Prog Polym Sci 16:303–329. https://doi.org/10.1016/0079-6700(91)90021-C

82. Busico V, Cipullo R, Monaco G et al (1999) New insight in propene polymerization promoted by heterogeneous Ziegler-Natta catalysts. In: Kaminsky W (ed) Metalorganic catalysts for synthesis and polymerization. Springer, Berlin, pp 76–88

83. Alamo RG, Kim M-H, Galante MJ et al (1999) Structural and kinetic factors governing the formation of the γ polymorph of isotactic polypropylene. Macromolecules 32:4050–4064. https://doi.org/10.1021/ma981849r

84. Auriemma F, De Rosa C (2002) Crystallization of metallocene-made isotactic polypropylene: disordered modifications intermediate between the α and γ forms. Macromolecules 35:9057–9068. https://doi.org/10.1021/ma020648r

85. De Rosa C, Auriemma F, Circelli T et al (2002) Crystallization of the α and γ forms of isotactic polypropylene as a tool to test the degree of segregation of defects in the polymer chains. Macromolecules 35:3622–3629. https://doi.org/10.1021/ma0116248

86. De Rosa C, Auriemma F, Spera C et al (2004) Comparison between polymorphic behaviors of Ziegler-Natta and metallocene-made isotactic polypropylene: the role of the distribution of defects in the polymer chains. Macromolecules 37:1441–1454. https://doi.org/10.1021/ma035295q

87. De Rosa C, Auriemma F, Spera C et al (2004) Crystallization properties of elastomeric polypropylene from alumina-supported tetraalkyl zirconium catalysts. Polymer 45:5875–5888. https://doi.org/10.1016/j.polymer.2004.06.037

88. Sundell T, Fagerholm H, Crozier H (1996) Isotacticity determination of polypropylene using FT-Raman spectroscopy. Polymer 37:3227–3231. https://doi.org/10.1016/0032-3861(96)88466-7

89. Zhu X, Yan D, Fang Y (2001) In situ FTIR spectroscopic study of the conformational change of isotactic polypropylene during the crystallization process. J Phys Chem B 105:12461–12463. https://doi.org/10.1021/jp012165f

90. Kissin YV, Tsvetkova VI, Chirkov NM (1972) The stereoregularity of polypropylene from IR and NMR data. Eur Polym J 8:529–546. https://doi.org/10.1016/0014-3057(72)90131-0

91. Kissin YV, Rishina LA (1976) Regularity bands in the I.R. spectra of C_3H_6-C_3D_6 copolymers. Eur Polym J 12:757–759. https://doi.org/10.1016/0014-3057(76)90088-4

92. Hsu SL, Hahn T, Suen W et al (2001) An analysis of Raman spectra of syndiotactic polypropylenes. 2. Configurational defects. Macromolecules 34:3376–3383. https://doi.org/10.1021/ma001448n

93. Sevegney MS, Kannan RM, Siedle AR et al (2006) Vibrational spectroscopic investigation of stereoregularity effects on syndiotactic polypropylene structure and morphology. Vib Spectrosc 40:246–256. https://doi.org/10.1016/j.vibspec.2005.10.003

94. Pasquini N (2005) Polypropylene handbook. Product, technology, market. Hanser, Munich

95. Xu J, Feng L (2000) Application of temperature rising elution fractionation in polyolefins. Eur Polym J 36:867–878. https://doi.org/10.1016/S0014-3057(99)00143-3

96. Amer I, van Reenen A (2009) Fractionation and crystallization of isotactic poly(propylenes) prepared with a heterogeneous transition metal catalysts. Macromol Symp 282:33–40. https://doi.org/10.1002/masy.200950804

97. Viville P, Daoust D, Jonas AM et al (2001) Characterization of the molecular structure of two highly isotactic polypropylenes. Polymer 42:1953–1967. https://doi.org/10.1016/S0032-3861(00)00529-2

98. Monrabal B (1996) Crystaf: crystallization analysis fractionation. A new approach to the composition analysis of semicrystalline polymers. Macromol Symp 110:81–86. https://doi.org/10.1002/masy.19961100107

99. Monrabal B (2006) Microstructure characterization of polyolefins. Tref and crystaf. In Shiono T, Nomura K, Terano M (eds) Studies in surface science and catalysis, vol 161, pp 35–42, Elsevier. https://doi.org/10.1016/S0167-2991(06)80431-3

100. Monrabal B, Sancho-Tello J, Mayo N et al (2007) Crystallization elution fractionation. A new separation process for polyolefin resins. Macromol Symp 257:71–79. https://doi.org/10.1002/masy.200751106

101. Virkkunen V, Laari P, Pitkänen P et al (2004) Tacticity distribution of isotactic polypropylene prepared with heterogeneous Ziegler–Natta catalyst. 2. Application and analysis of SSA data for polypropylene. Polymer 45:4623–4631. https://doi.org/10.1016/j.polymer.2004.05.027

102. Kang J, Yang F, Wu T et al (2012) Polymerization control and fast characterization of the stereo-defect distribution of heterogeneous Ziegler–Natta isotactic polypropylene. Eur Polym J 48:425–434. https://doi.org/10.1016/j.eurpolymj.2011.11.023

103. Alt HG, Köppl A (2000) Effect of the nature of metallocene complexes of group IV metals on their performance in catalytic ethylene and propylene polymerization. Chem Rev 100:1205–1222. https://doi.org/10.1021/cr9804700

104. Kaminsky W, Funck A, Hähnsen H (2009) New application for metallocene catalysts in olefin polymerization. Dalton Trans 8803–8810. https://doi.org/10.1039/B910542P

105. Domski GJ, Rose JM, Coates GW et al (2007) Living alkene polymerization: new methods for the precision synthesis of polyolefins. Prog Polym Sci 32:30–92. https://doi.org/10.1016/j.progpolymsci.2006.11.001

106. Harney MB, Zhang Y, Sita LR (2006) Discrete, multiblock isotactic-atactic stereoblock polypropene microstructures of differing block architectures through programmable stereomodulated living Ziegler-Natta polymerization. Angew Chem Int Edit 45:2400–2404. https://doi.org/10.1002/anie.200600027

107. Talarico G, Busico V, Cavallo L (2004) "Living" propene polymerization with bis (phenoxyimine) Group 4 metal catalysts: new strategies and old concepts. Organometallics 23:5989–5993. https://doi.org/10.1021/om049296y

108. Busico V, Cipullo R, Friederichs N et al (2004) Block copolymers of highly isotactic polypropylene via controlled Ziegler-Natta polymerization. Macromolecules 37:8201–8203. https://doi.org/10.1021/ma048144b

109. Gottfried AC, Brookhart M (2003) Living and block copolymerization of ethylene and α-olefins using palladium(ii)-a-diimine catalysts. Macromolecules 36:3085–3100. https://doi.org/10.1021/ma025902u

110. Busico V, Cipullo R, Friederichs N et al (2003) The first molecularly characterized isotactic polypropylene-block-polyethylene obtained via "quasi-living" insertion polymerization. Macromolecules 36:3806–3808. https://doi.org/10.1021/ma0342527

111. Tshuva EY, Goldberg I, Kol M et al (2001) Living polymerization and block copolymerization of α-olefins by an amine bis(phenolate) titanium catalyst. Chem Commun 2120–2121. https://doi.org/10.1039/B105492A

112. Mitani M, Nakano T, Fujita T (2003) Unprecedented living olefin polymerization derived from an attractive interaction between a ligand and a growing polymer chain. Chem-Eur J 9:2396–2403. https://doi.org/10.1002/chem.200304661

113. Weberski MP, Chen C, Delferro M et al (2012) Suppression of β-hydride chain transfer in nickel(ii)-catalyzed ethylene polymerization via weak fluorocarbon ligand–product interactions. Organometallics 31:3773–3789. https://doi.org/10.1021/om3002735

114. Bates FS, Fredrickson GH (1990) Block copolymer thermodynamics: theory and experiment. Annu Rev Phys Chem 41:525–557. https://doi.org/10.1146/annurev.pc.41.100190.002521

115. Cheng JY, Mayes AM, Ross C (2004) Nanostructure engineering by templated self-assembly of block copolymers. Nat Mater 3:823–828. https://doi.org/10.1038/nmat1211

116. Stoykovich MP, Müller M, Kim SO et al (2005) Directed assembly of block copolymer blends into nonregular device-oriented structures. Science 308:1442–1446. https://doi.org/10.1126/science.1111041

117. De Rosa C, Auriemma F, Di Girolamo R et al (2010) Enabling strategies in organic electronics using ordered block copolymer nanostructures. Adv Mater 22:5414–5419. https://doi.org/10.1002/adma.201002649

118. Eagan JM, Xu J, Di Girolamo R et al (2017) Combining polyethylene and polypropylene: enhanced performance with PE/iPP multiblock polymers. Science 355:814–816. https://doi.org/10.1126/science.aah5744

119. Valente A, Mortreux A, Visseaux M et al (2013) Coordinative chain transfer polymerization. Chem Rev 113:3836–3857. https://doi.org/10.1021/cr300289z

120. Arriola DJ, Carnahan EM, Hustad PD et al (2006) Catalytic production of olefin block copolymers via chain shuttling polymerization. Science 312:714–719. https://doi.org/10.1126/science.1125268

121. Rose JM, Cherian AE, Coates GW (2006) Living polymerization of α-olefins with an α-diimine ni(ii) catalyst: formation of well-defined ethylene-propylene copolymers through controlled chain-walking. J Am Chem Soc 128:4186–4187. https://doi.org/10.1021/ja058183i

122. Lamberti M, Mazzeo M, Pappalardo D et al (2009) Mechanism of stereospecific polymerization of α-olefins by late-transition metal and octahedral group 4 metal catalysts. Coordin Chem Rev 253:2082–2097. https://doi.org/10.1016/j.ccr.2009.02.014